Yang, S., Horsfield, B., Mahlstedt, N., Stephenson, M., Könitzer, S. (2016): On the primary and secondary petroleum generating characteristics of the Bowland Shale, northern England. - *Journal of the Geological Society London*, *173*, 2, pp. 292—305.

DOI: http://doi.org/10.1144/jgs2015-056

JGS
Journal of the Geological Society

Research article

Published Online First

doi:10.1144/jgs2015-056

# On the primary and secondary petroleum generating characteristics of the Bowland Shale, northern England

**S. Yang[1*], B. Horsfield[1], N. Mahlstedt[1], M. Stephenson[2] & S. Könitzer[3]**

[1] *HelmholtzCentrePotsdam* GFZ German Research Centre for Geosciences, Telegrafenberg, 14473 Potsdam, Germany
[2] British Geological Survey, Keyworth, Nottingham NG12 5GG, UK
[3] Department of Geology, University of Leicester, University Road, Leicester LE1 7RH, UK
* Correspondence: henryyang@gfz-potsdam.de

**Abstract:** The Carboniferous Bowland Shale of northern England has drawn considerable attention because it has been estimated to have 1329 trillion cubic feet hydrocarbons in-place (gas and liquids) resource potential (Andrews 2013). Here we report on the oil and gas generation characteristics of three selected Bowland Shale whole-rock samples taken from cores and their respective kerogen concentrates. Compositional kinetics and phase properties of the primary and secondary fluids were calculated through the PhaseKinetics and GOR-Fit approaches and *PVT* modelling software. The three Bowland Shale samples contain immature, marine type II kerogen. Pyrolysate compositions imply primary generation of paraffinic–naphthenic–aromatic (PNA) oil with low contents of wax and sulphur. Bulk kinetic parameters have many similarities to those of productive American Palaeozoic marine shale plays. The secondary gas generation potential of Bowland Shale is greater than the primary gas potential although it requires a 10 kcal $mol^{-1}$ higher activation energy to achieve peak production. Primary oil, primary gas and secondary gas reach their maximum generation at 137, 150 and 200°C respectively for a 3°C $Ma^{-1}$ heating rate. Different driving forces of expulsion including the generation of hydrocarbon and overpressure caused by phase separation during sequential periods of subsidence and uplift could be inferred.

**Received** 6 May 2015; **revised** 17 September 2015; **accepted** 22 September 2015

It was in the 1980s that Selley (1987) drew attention to the high shale gas potential of organic-rich shales in the UK (Selley 1987, 2005; Smith 1995). He suggested that the most prospective candidates were the Lower Carboniferous basins in northern Britain. Concerted exploration with a view to exploitation was never seriously considered until 20 years or so later, when horizontal drilling and hydraulic fracturing revolutionized unconventional gas production in the USA and directly led to the rapid emergence of the shale gas industry (Curtis 2002; Bowker 2007; Pollastro 2007). Indeed, it was after the UK's 13th Onshore Licensing Round in 2008 that companies and government made a concerted effort in shale gas assessment and exploration (DECC 2011). USEIA (2011) evaluated that the Bowland Shale system possesses a risked GIP of 95 trillion cubic feet (tcf) and made a risked recoverable resource estimate of 19 tcf. Gas-in-place has been estimated by the British Geological Survey (BGS) to lie in the range 822–2281 tcf (Andrews 2013). Known as a conventional source rock in the Bowland Basin and elsewhere in northern England (Lawrence *et al.* 1987), the Carboniferous Bowland Shale is also the prime shale gas target in the UK (Smith *et al*. 2010; Selley 2012). The first UK shale gas well (Preese Hall No. 1), drilled by Cuadrilla Resources in 2010, targeted the play as having the highest shale gas potential in the country (Green *et al.* 2012).

The integration of outcrop, well and seismic data has shown that the Bowland Shale can be divided into lower and upper parts. The upper Bowland Shale is thinner but possesses a higher organic matter content and exhibits better lateral continuity than the lower part (Andrews 2013). The organic-rich upper part of the Bowland Shale is hemi-pelagic in origin and is dominated by clay-rich mudstone intercalated with very thin calcareous mudstones (Chisholm *et al.* 1988). The average thickness of this formation is 150 m (locally reaching 890 m). The upper Bowland Shale, the focus of the current investigation, was deposited in several adjoining basins (Widmerpool Gulf, North Staffordshire Basin, Edale Basin, etc.) separated by the emergent East Midlands Shelf (Fig. 1). The lower shale layer (age from late Chadian to Brigantian), which was interbedded with mass-flow limestones and sandstones (Waters *et al*. 2009), is considerably thicker, reaching 3000 m in its depocentres (Andrews 2013). The sedimentology and structural geology of the Bowland Shale have been studied by many researchers (Lawrence *et al.* 1987; Barrett 1988; Leeder 1988; Fraser & Gawthorpe 2003; Waters *et al.* 2009). Biomarkers and stable carbon isotopes have established likely precursor biota of the organic matter (Ewbank *et al.* 1993; Armstrong *et al.* 1997). Also, Könitzer *et al*. (2014) have used total organic carbon (TOC) and carbon isotope composition to differentiate various depositional environments vertically.

The mass of in-place gas can be evaluated using a combination of forward (including kinetic) and inverse (including mass-balance) modelling. Because shales are extremely heterogeneous (Jarvie *et al.* 2007), both laterally (tens to hundreds of kilometres) and vertically (metres to decimetres), the exploration equation has to be applied at appropriate intervals for regional- and reservoir-scale applications. The degree to which the *in situ* potential can be realized (trr) is mainly determined by the effectiveness of hydraulic fracturing at test sites.

To date, mainly inverse modelling has been applied to the Bowland Shale; thus, its shale gas potential (Selley 2005, 2012; Smith *et al.* 2010; Raji 2013) and total energy resource potential (DECC 2011; USEIA 2011; Andrews 2013; Hough & Vane 2014) have been calculated using basic geochemical data, including TOC and Rock-Eval. Gross *et al*. (2014) concluded that the high average TOC content and large thicknesses of the mudstone lithofacies point to a significant shale gas and liquid potential in areas with appropriate maturity (1.2–3.5% $R_o$), but a relatively low average hydrogen index (HI) and high clay content may be seen as detrimental to shale gas potential. Concerning trr, de Pater & Baisch

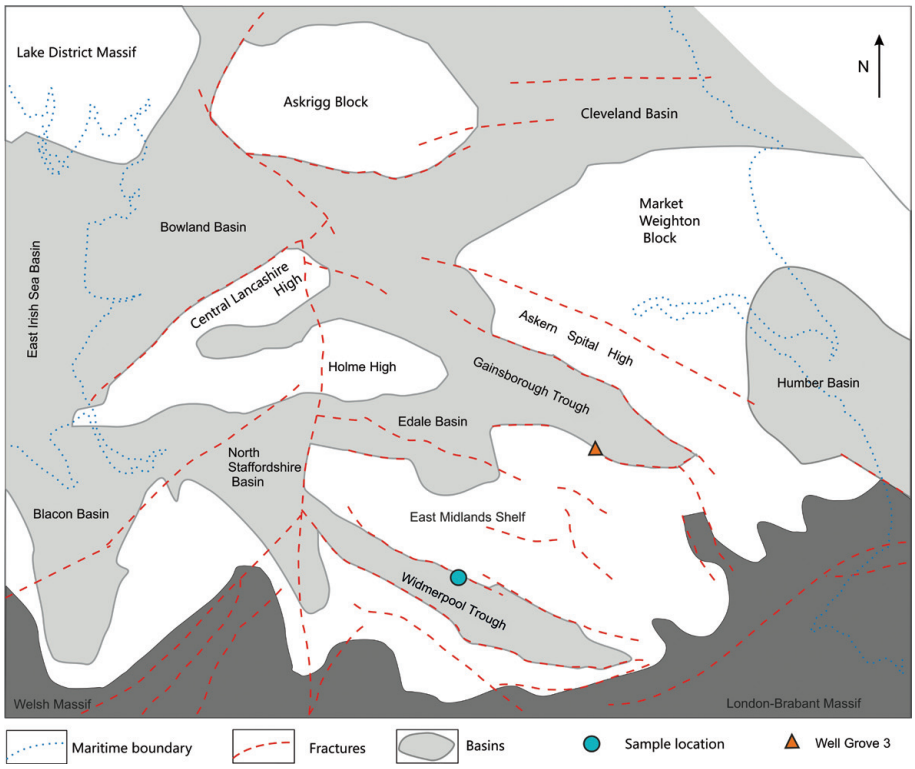


**Fig. 1.** Locations of samples and 1D basin modelling well. Namurian basin distribution after Fraser and Gawthorpe (2003).

(2011), Green *et al*. (2012) and Imber *et al*. (2014) have recently documented the orientation of fractures in the Bowland Shale and evaluated the formation's frackability (the ease with which the rock can be fractured) using rock mechanical experiments and seismic data. The Bowland Shale consists mainly of impermeable, brittle rock (varying according mineralogy), with many faults and fractures. The maximum horizontal stress orientation of 8°NNW agrees with the regional stress distribution.

Little or no kinetics-related work has been published on the Bowland Shale, neither on 'conversion' using bulk kinetics nor on 'per cent gas' using compositional kinetics or physical property prediction, as a function of organic matter type and/or facies (see exploration equation). Kinetics models basically describe the 'ease' with which the substituents in the kerogen break down to form hydrocarbons via assumed pseudoreactions (Braun & Burnham 1987; Burnham *et al.* 1988; Schenk *et al.* 1997). Utilizing specific kinetic parameters for the target shale is imperative whenever possible (Dieckmann & Keym 2006; Peters *et al*. 2006). Compositional kinetics provides compositional information on the generated fluids; surface gas–oil ratio (GOR) and gas dryness prediction are of great importance, because both of them have a major influence on the quality of the produced oil and gas. The PhaseKinetics model characterizes the compositional evolution of the fluids generated with increasing thermal stress, as well as the phase behaviour of the petroleum at different maturity levels (Di Primio & Horsfield 2006). Predictions of bulk petroleum compositions and physical properties have already been published for basins in South Africa (Hartwig *et al.* 2012), North Dakota (Kuhn *et al*. 2012), Norway (Rodrigues Duran *et al.* 2013), eastern Canada (Baur *et al.* 2010), Brazil (Di Primio & Horsfield 2006) and China (Tan *et al*. 2013), in several cases with confirmation of the prediction using local calibration. In the current study we employed the PhaseKinetics approach on both whole-rock samples and kerogen concentrates to predict the properties of fluids generated from Bowland Shale, also taking into consideration the impact of rock–fluid interactions (mineral matrix effects, considered to be laboratory artefects) on the results (see Espitalie *et al*. 1980; Horsfield & Douglas 1980).

The contribution of secondary gas at high levels of thermal stress, determined to be dominant in the majority of shale gas 'sweet spots' (Jarvie *et al.* 2007), also needs to be qualitatively and quantitatively evaluated. The GOR-Fit model Mahlstedt *et al*. (2013) discriminates between primary gas, primary oil (both from kerogen breakdown) and secondary gas (from the breakdown of primary oil), and has been successfully applied to marine and lacustrine shales in Germany (Ziegs 2013). In the current study we employed the GOR-Fit kinetic model to predict secondary gas formation in the Bowland Shale.

Here, we have focused on the specific kinetic parameters themselves, utilizing a 1D basin model to demonstrate how fluid properties change as a function of organic maturity and reservoir conditions. We have then considered the evolution of expulsion mechanisms during different geological times, and considered the degree of secondary gas formation, comparing our model with default kinetics models derived from published studies in Petromod©.

## Samples and analytical procedure

### *Samples*

The shallow Carsington Dam Reconstruction C4 borehole (SK 244 503), which targeted upper Bowland Shale, was drilled in Derbyshire, northern England. Both hemi-pelagic marine shale and pro-deltaic turbiditesdeposited in deep-basin waterwere recognized using micropetrography and TOC-bulk $\delta^{13}C_{org}$ data (Könitzer *et al.* 2014). Thick intervals of marine Bowland Shale are relatively homogeneous on a metre scale, whereas intervals of interbedded shales and turbiditic sandstones are relatively more heterogeneous, as revealed by petrophysical (Hough & Vane 2014), geochemical (Gross *et al.* 2014) and lithological (Könitzer *et al.* 2014) properties. Three unweathered core shale samples as well as their kerogen concentrates from the marine part of the well were tested in this study. Thin-section observation and mineralogy had previously shown that samples 1 and 3 represent thin-bedded carbonate-bearing clay-rich mudstones and sample 2 is lenticular clay-dominated mudstone. All three samples have $\delta^{13}C_{org}$ values between −28.0 and −28.4‰, indicating that the kerogen is derived

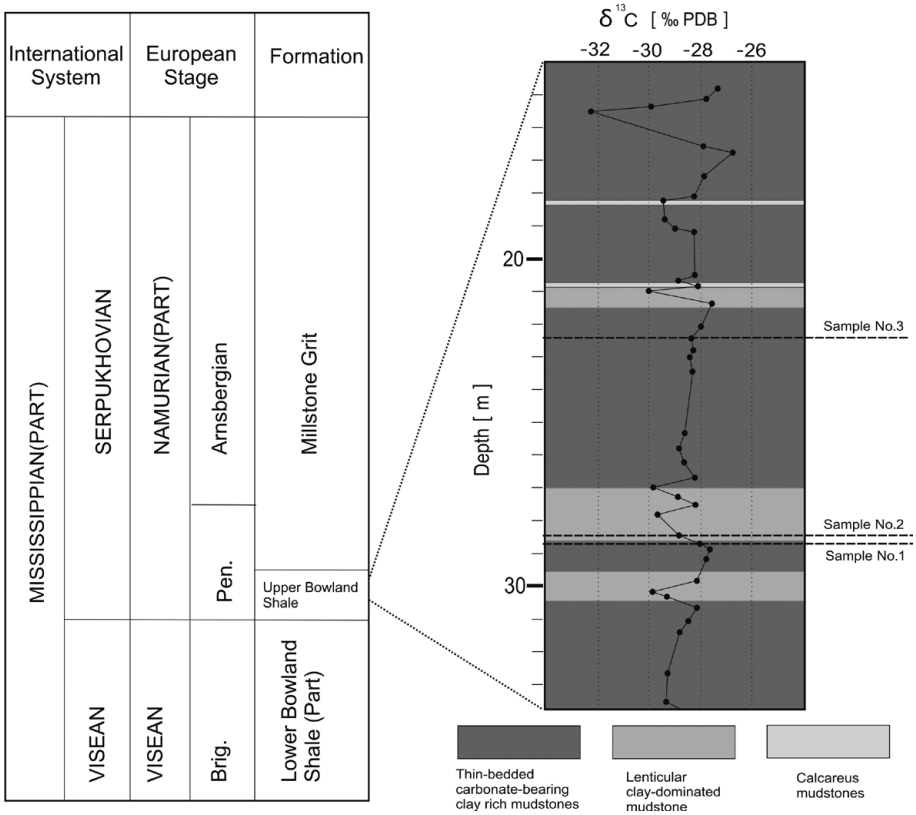


**Fig. 2.** Stratigraphy of the study area, showing depth, lithology and bulk $\delta^{13}C_{org}$ data of the Carsington C4 core samples (Könitzer *et al*. 2014) as well as the locations of the three shale samples investigated in this paper.

from marine planktonic algae, so the three samples are representative of the thick hemi-pelagic mudstones, the dominant lithofacies in the succession at Carsington (Fig. 2; Könitzer *et al.* 2014).

### *Analytical procedure*

#### *Kerogen isolation and screening*

Kerogen concentrates were obtained by (1) crushing the shale to millimetre size, (2) treating with hydrofluoric acid for 1 week at room temperature and (3) sieving to 10–500 μm. TOC and Rock-Eval analyses were performed using a Leco SC-632 Analyser and Rock-Eval 6 instrument respectively, following established procedures (Espitalié *et al.* 1977).

#### *PhaseKinetics (compositional kinetics)*

The PhaseKinetics approach of Di Primio & Horsfield (2006) has four stages, as follows.

(1) Pyrolysis–gas chromatography (PyGC), providing a quick evaluation of the kerogen structure characteristics in terms of petroleum type organofacies, was performed using a Quantum MSSV-2 Thermal Analysis System® interfaced with an Agilent GC-6890A (Horsfield *et al.* 2015). Briefly stated, milligram quantities (whole-rock 14–16 mg; kerogen 2–4 mg) of each sample were loaded into a small open glass tube and heated under flowing helium; free hydrocarbons were vented for 3 min during an isothermal purge at 300°C, after which the $C_{2+}$ pyrolysis products generated during heating from 300 to 600°C were collected in a cryogenic trap (liquid nitrogen). Methane passed through the trap and passed through the GC column to the Flame Ionisation Detector (FID).Trapped products were liberated by removing the cooling agent and heating the trap to 300°C. An AHP-Ultra 1 dimethylpolysiloxane capillary column (50 m length, inner diameter 0.32 mm, film thickness 0.52 mm) connected to an FID was used with helium as carrier gas. Quantification of single compounds and boiling range splits was conducted by external standardization with *n*-butane.

(2) Bulk kinetic parameters were assessed by subjecting samples to open-system, non-isothermal pyrolysis at four linear heating rates (0.7, 2, 5 and 15°C $min^{-1}$) using a Source Rock Analyser® (SRA), following established procedures (Braun & Burnham 1987). The discrete activation energy ($E_a$) distribution optimization with a single, variable frequency factor ($A$) as well as geological extrapolation were performed using the KINETICS 2000® and KMOD® programs (Burnham *et al.* 1987).

(3) Non-isothermal closed-system microscale sealed vessel (MSSV) pyrolysis (Horsfield *et al*. 1989) is a micro-analytical method to artificially mature sedimentary organic matter to different stages of conversion and to quantify the composition of generated products. It provides the possibility of determining primary and secondary reaction kinetics of specific compound groups and to extrapolate their generation to geological heating rates (Horsfield *et al.* 2015). For each experiment, milligram quantities of samples were sealed in glass capillaries and artificially matured at 0.7°C $min^{-1}$ to temperatures corresponding to a transformation ratio (TR) of 10, 30, 50, 70 and 90% as defined by bulk kinetic results. The tubes were then cracked open using a piston device coupled with the injector, and the released products were swept into the GC system using a flow of helium. Quantification was performed by external standardization using *n*-butane.

(4) The final step consists of compositional kinetics determination and physical property modelling. The hydrocarbons generated during MSSV are divided into 14 pseudo-compositions. Seven of them are in the gas fraction ($C_1$, $C_2$, $C_3$, *i*-$C_4$, *n*-$C_4$, *i*-$C_5$, *n*-$C_5$) and the gas composition was corrected based on a GOR–gas-wetness correlation from natural black oil. The other seven compounds describe the liquid phase consisting of $C_6$ and pseudo-boiling ranges of $C_{7–15}$, $C_{16–25}$, $C_{26–35}$, $C_{36–45}$, $C_{46–55}$ and $C_{56–80}$. According to the weight percentage of the 14 pseudo-compositions, each bulk kinetic potential that has the same activation energy was populated into 14 parts; these compositional kinetics models are then ready to be applied to basin modelling software (especially the IES PetroMod®, which has a module for inputting these), which makes

**Table 1.** *Rock-Eval and TOC data*

| Sample number | GFZ number | Depth (m) | $S_1$ (mg g$^{-1}$) | $S_2$ (mg g$^{-1}$) | $S_3$ (mg g$^{-1}$) | $T_{max}$ (°C) | HI (mg HC g$^{-1}$ TOC) | OI (mg $CO_2$ g$^{-1}$ TOC) | PI ($S_1/(S_1 + S_2)$) | TOC (%) |
|---|---|---|---|---|---|---|---|---|---|---|
| Whole-rock 1 | G013218 | 28.68 | 0.18 | 1.71 | 1.67 | 429 | 62 | 61 | 0.0952 | 2.75 |
| Whole-rock 2 | G013219 | 28.42 | 0.16 | 4.88 | 0.7 | 438 | 188 | 27 | 0.0317 | 2.6 |
| Whole-rock 3 | G013220 | 22.36 | 0.37 | 6.46 | 0.49 | 430 | 206 | 16 | 0.0542 | 3.14 |
| Kerogen 1 | G013688 | 28.68 | 1.36 | 60.89 | 1.20 | 430 | 329 | 6 | 0.0218 | 18.5 |
| Kerogen 2 | G013689 | 28.42 | 0.39 | 14.13 | 0.48 | 432 | 318 | 11 | 0.0269 | 4.45 |
| Kerogen 3 | G013690 | 22.36 | 1.18 | 33 | 0.83 | 426 | 324 | 8 | 0.0345 | 10.2 |

GFZ: GeoForschungZentrum. $S_1$: quantity of free hydrocarbons (gas + oil). $S_2$: quantity of thermally generated (cracked) hydrocarbons. $S_3$: quantity of $CO_2$ generated during pyrolysis of the sample. HI (hydrogen index)=($S_2$*100)/TOC. OI (oxygen index)=($S_3$*100)/TOC. PI (production index) = $S_1/(S_1+S_2)$

this method very convenient. Physical property modelling was carried out using PVT-Sim® based on the 14 pseudo-compounds determined by MSSV. Standard temperature and pressure (STP) GOR was calculated through the separator simulator module in the software and phase envelopes were also drawn.

### *GOR-Fit*

The GOR-Fit model based on open-system SRA and closed-system MSSV pyrolysis consists of three main steps (Mahlstedt *et al.* 2013). In the first step, the MSSV generation of $C_{1-5}$, $C_{6+}$ and the total $C_{1+}$ boiling fractions is normalized to the maximum MSSV yields. Because the normalized $C_{1+}$ MSSV yields curve and SRA–TR curves are identical (Schenk & Horsfield 1993) and only primary cracking takes place in the open-system the SRA pyrolysis, the primary oil and gas splines can be deduced from the SRA–TR curve by multiplying by an oil and gas ratio assumed fixed and derived from pyrolysis gas chromatography after a small temperature adjustment to fit the measured MSSV oil and gas generation curves better. The second step is to calculate the secondary gas amount by subtracting primary gas from measured MSSV oil yields at corresponding temperatures. A secondary gas spline is again approximated by 'factorizing' the SRA curve (using a factor derived from multiplication of the $C_{6+}$ spline factor by 0.7 assuming that 70% of $C_{6+}$ compounds are degraded to gas and 30% to coke), which is then temperature shifted to match calculated secondary gas yields. After obtaining the generation characteristics of primary oil, primary gas and secondary gas at three heating rates, the kinetics models and geological extrapolations were achieved by using KINETICS 2000® and KMOD® in the final step.

### *1D basin modelling*

One-dimensional basin modelling was carried out on well Grove 3 of the East Midlands Shelf using IES PetroMod®2013. Lithology and depth inputs in the modelling came from the drilling, and stratigraphic ages were taken from Gradstein *et al*. (2004) and International Commission on Stratigraphy (Cohen *et al.* 2014). A kerogen–oil–gas kinetics model with secondary reaction developed on kerogen 3 in this study was used as kinetics input. Two periods of uplift of the Bowland Shale, in the late Carboniferous/early Permian and after the Late Cretaceous, have been recognized by Barrett (1988) and Leeder (1988), and the heat flow model was modified after Jarvis & McKenzie (1980). Calibration on vitrinite reflectance is in accordance with a BGS report, which also described 1D modelling on well Grove 3 (Andrews 2013).

## Results and discussion

### *Primary generation*

Here we compare the results for whole-rock samples with those for kerogen concentrates. Significant differences in composition are reported, the causes are discussed, and the ramifications for petroleum composition are outlined.

### *Whole-rock*

All three whole-rock samples have TOC contents higher than 2% (Table 1), fitting the minimum TOC requirement for shale gas development (Curtis 2002; Muntendam-Bos 2009), but the $S_2$ and HI values are low (Table 1). Rock-Eval crossplots confirm that the three whole-rock samples generate and release pyrolysates with a type III composition (Fig. 3a). Samples 1 and 3 are immature samples whereas sample 2 is marginally mature (Fig. 3b).

In cases where analytical artefacts are excluded (e.g. mineral–organic interactions occurring during pyrolysis; Horsfield & Douglas 1980) the proportion of resolved and identifiable compounds in the GC trace reflects the kerogen structure as a whole (Larter 1984; Horsfield 1989). Their GC traces show that the whole-rock samples analysed here tend to generate high percentages of low molecular weight compounds ($C_1$–$C_5$) and high concentrations of aromatic compositions such as ethylbenzene, xylenes, trimethylbenzene and naphthalene (Fig. 4). The average alkyl chain length distributions (Horsfield 1989, 1997) of the pyrolysates from whole-rocks 1 and 3 are of the gas and condensate type whereas whole-rock 2 falls in the low wax paraffinic–naphthenic–aromatic (PNA) crude oil field (Fig. 5). Two additional ternary diagrams were used to characterize the pyrolysate in terms of aromaticity, paraffinicity and either sulphur content (Eglinton *et al.* 1990) or phenol content (Larter 1984). They clearly show that the whole-rock pyrolysate is very aromatic (Fig. 6a and b); sulphur-containing compounds and phenols are in low abundance (Fig. 6a and b).

As far as thermal response is concerned, whole-rock Bowland Shales have peak activation energies between 55 and 57 kcal mol$^{-1}$ and frequency factors exceed $2.85 \times 10^{14}$ (Fig. 7). Applying these values to natural maturation using a typical geological heating rate (3°C Ma$^{-1}$), the whole-rock samples 1 and 3 reach 50% TR at about 150°C (Fig. 8), whereas whole-rock sample 2 needs around 10° more to reach that TR. These kinetics characteristics of the whole-rock samples are unusual, in that the samples require higher temperatures for kerogen breakdown than most known Palaeozoic marine shales (e.g. Mahlstedt 2012).

Two compositional kinetics models for whole-rock samples are shown in Figure 9. These were constructed by populating the bulk kinetic potentials with MSSV pyrolysis data (after Di Primio & Horsfield 2006). Cumulative GORs in the surface environment of whole-rock samples are enhanced with increasing thermal maturation except for two slightly deviant values from samples 1 and 2 at 50% TR (Fig. 10). The maximum GOR can be as high as 498 m$^3$ Sm$^{-3}$ for sample 1 at 90% TR, which is very similar to the GOR behaviour of Arang coal (organic type III) of Indonesia (Di Primio & Horsfield 2006). The pressure–temperature phase envelope for a multicomponent mixture gives the region of temperatures and pressures at which the mixture forms two phases. Generally speaking, the envelope in the temperature axis direction is controlled by molecular weight, whereas GOR and gas wetness control the pressure axis direction (Amyx *et al.* 1960). Phase

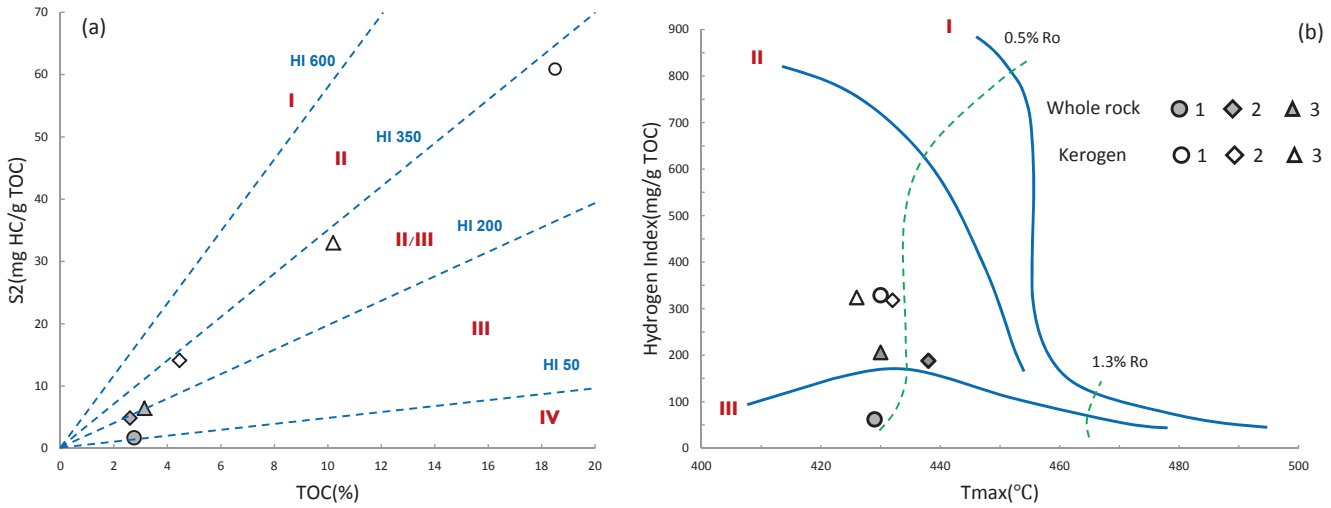


**Fig. 3.** Rock-Eval and TOC diagrams for kerogen type and maturity identification.

envelopes of whole-rock sample 3 reflect the fact that the primary generated fluids are dominated by low molecular weight compounds (Fig. 11). For a hypothetical reservoir at 100°C and 200 bar, the critical point of hydrocarbons accumulating up to 90% TR is very close to that reservoir condition, and the fluids can be termed volatile oil (McCain 1990).

### *Kerogen*

Although the three kerogen concentrates have different TOC contents and $S_2$ values (Table 1), they share very similar HIs. With an HI range of 318–329 mg HC $g^{-1}$ TOC the three kerogen concentrates are classified as type II (Fig. 3a). The maturity indicator $T_{max}$ implies that the three kerogen concentrates are immature (Fig. 3b).

The pyrolysates of kerogen are dominated by normal alkanes or alkenes, and subsidiary aromatics and other resolved peaks are generated (Fig. 4). All three concentrates fall in the low-wax PNA oil area (Fig. 5), which indicates the typical characteristics of many marine shales (Horsfield 1997). Figure 6 suggests that hydrocarbons generated by kerogen are richer in paraffinic compounds than aromatic ones. In addition, the sulphur content is also very low (Fig. 6a).

Peak activation energies of the three kerogen concentrates are 51 kcal $mol^{-1}$ and their frequency factors range from $1.54 \times 10^{13}$ to $2.42 \times 10^{13}$ (Fig. 7). The geological extrapolation curves plot close together as regards TR variations according to temperature (Fig. 8). The Bowland Shale kerogen generation kinetics is more stable than that of sulphur-rich marine shale (Dieckmann 2005) and closely resembles results reported for productive unconventional shale plays from the USA including Barnett Shale (Jarvie *et al.* 2010), Bakken Shale (Kuhn *et al*. 2012) and Woodford Shale (Mahlstedt 2012).

Owing to the limited amount of sample available, MSSV experiments were not carried out on kerogen 2. Compositional kinetics results of samples 1 and 3 show that about half of the hydrocarbons in peak generation (activation energies range between 50 and 54 kcal $mol^{-1}$) are contributed by compounds between $C_7$ and $C_{25}$ and gases make up only small proportions of the total products (Fig. 9).

Cumulative GOR variations as a function of increasing TR for kerogens 1 and 3 are closely similar (Fig. 10). GOR increases steadily from less than 100 $m^3$ $Sm^{-3}$ at 10% TR to about 200 $m^3$ $Sm^{-3}$ at the highest TR, and this GOR variation pattern is very similar to those of the Woodford Shale and Kimmeridge Clay (Di Primio & Horsfield 2006). The cumulative hydrocarbon phase envelopes imply that fluids generated by Bowland kerogen concentrates are typical black oil (McCain 1990) and the systematic decrease in cricondentherms and increase in cricondenbars together with the shift of the critical point towards higher pressures and lower temperatures with increasing TR (Fig. 11) are consistent with pathways of critical point shifts of fluids from the Ekofisk, Eldfisk and Snorre Fields during maturation (Di Primio *et al.* 1998).

### *Comparison and discussion*

Clearly, there are significant compositional differences between the respective pyrolysates of whole-rock and kerogen concentrate pairs. The whole-rock samples show low HI values and are classified as containing type III organic matter, whereas the kerogen concentrates have higher HI and are classified as comprising type II organic matter (Fig. 3). Whole-rock samples tend to generate higher percentages of low molecular weight compounds ($C_1$–$C_5$) and alkylaromatics (Fig. 4), whereas the equivalent kerogen pyrolysate is dominated by normal alkanes and alkenes (Fig. 4). Ternary plots also demonstrate differences of organic facies and paraffinicity between these two materials (Figs 5 and 6). From the kinetic perspective, whole-rock samples are more refractory and heterogeneous than the kerogen (Figs 7 and 8). More light compounds were generated during pyrolysis from whole-rock samples, which is responsible for the higher GORs (Fig. 10) and lower cricondentherms in the phase envelopes (Fig. 11) than their kerogen counterparts.

The differences between kerogen and whole-rock pyrolysates have been discussed over decades. Saxby (1970) and Robl & Davis (1993) reported that the treatment of whole-rock by hydrofluoric acid during mineral dissolution and kerogen concentration does not change kerogen structure significantly. Differences in pyrolysate compositions have been attributed to the mineral matrix effect. This effect occurs in many open- and closed-system pyrolysis experiments including Rock-Eval (Espitalie *et al*. 1980, 1984; Senga-Makadi 1982), pyrolysis–GC (Horsfield & Douglas 1980; Karabakan & Yürüm 1998), bulk kinetics determination (Dembicki 1992; Burnham 1994; Pelet 1994; Dessort *et al*. 1997) and hydrocarbon expulsion efficiency calculations (Lewan *et al.* 2014), and is brought about by sorption followed by catalytic thermal degradation. Because of their high surface area (Sing 1985), clay minerals (especially smectite) have the ability to strongly adsorb pyrolysate (Espitalie *et al.* 1980, 1984), especially the heavy compounds (Katz 1983). Clay minerals tend to catalyse the kerogen to generate more $CO_2$, light hydrocarbons and aromatic compounds (Espitalié *et al*. 1984; Larter 1984; Tannenbaum *et al*. 1986; Lu *et al*. 1989). A disproportionation of hydrogen occurs in the

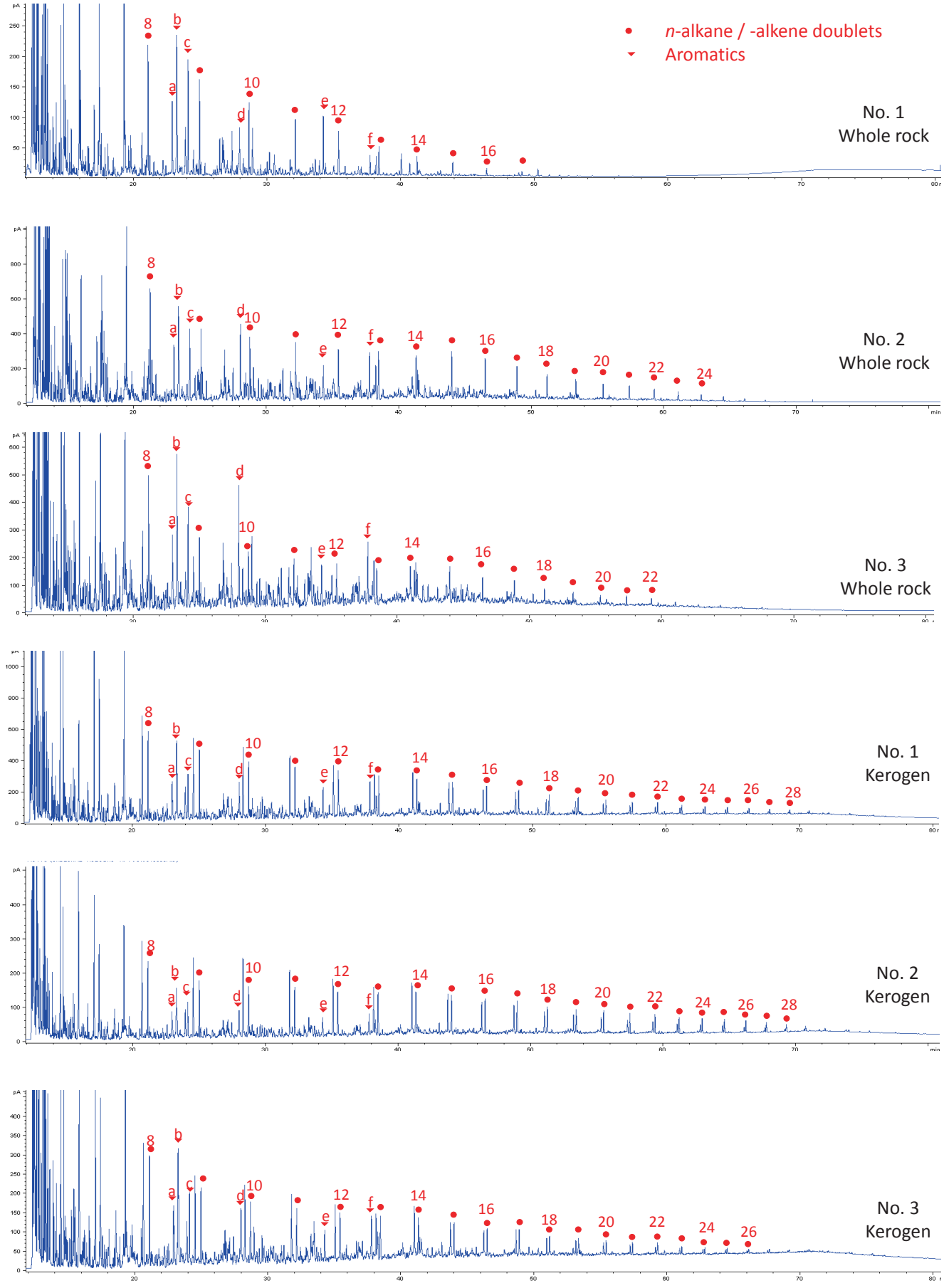


**Fig. 4.** PyGC chromatograms of the six samples. Normal alkane and alkene peaks have been highlighted and selectively numbered. Representative aromatic compounds are ethylbenzene (a), meta- and paraxylenes (b), orthoxylene (c), 1,2,4-trimethylbenzene (d), naphthalene (e) and 2-methylnaphthalene (f).

pyrolyser, enhancing $C_1$–$C_5$ yield while simultaneously depositing dead carbon, bringing about diminished HIs and lower yields of heavy compounds in Py-GC data, and being more refractory from a kinetic perspective. The overall outcome as far as bulk petroleum is concerned is that genetic potential is diminished (Figs 3 and 6), inherent oil potential is lowered relative to gas and in absolute terms (Figs 5 and 10), and phase envelopes change their shape accordingly (Fig. 11).

Sedimentological, organic petrological and stable carbon isotope studies (Armstrong *et al*. 1997; Fraser & Gawthorpe 2003; Könitzer *et al*. 2014) have shown that the upper Bowland Shale in this study is marine shale from predominantly hemi-pelagic deposition and organic matter is derived from planktonic phytoclasts. These attributes are better represented by the isolated kerogen pyrolysis data (Rock-Eval, PyGC and bulk kinetic results) than by the equivalent whole-rock data. It should be pointed out that the mineral matrix effects shown here are thought to exist only in artificial pyrolysis experiments and not during natural catagenesis. Fast heating rates, high temperatures, a dry pyrolysis environment and enhanced contact of the organic matter with minerals after grinding are considered as the main reasons that lead to the mineral matrix effect in laboratory pyrolysis (Senga-Makadi 1982; Vandenbroucke & Largeau 2007). Another important point is that

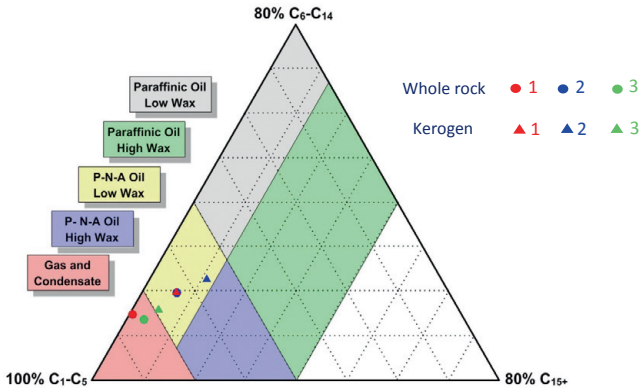


**Fig. 5.** Pyrolysate chain length distribution and petroleum type organofacies classification (Horsfield 1989).

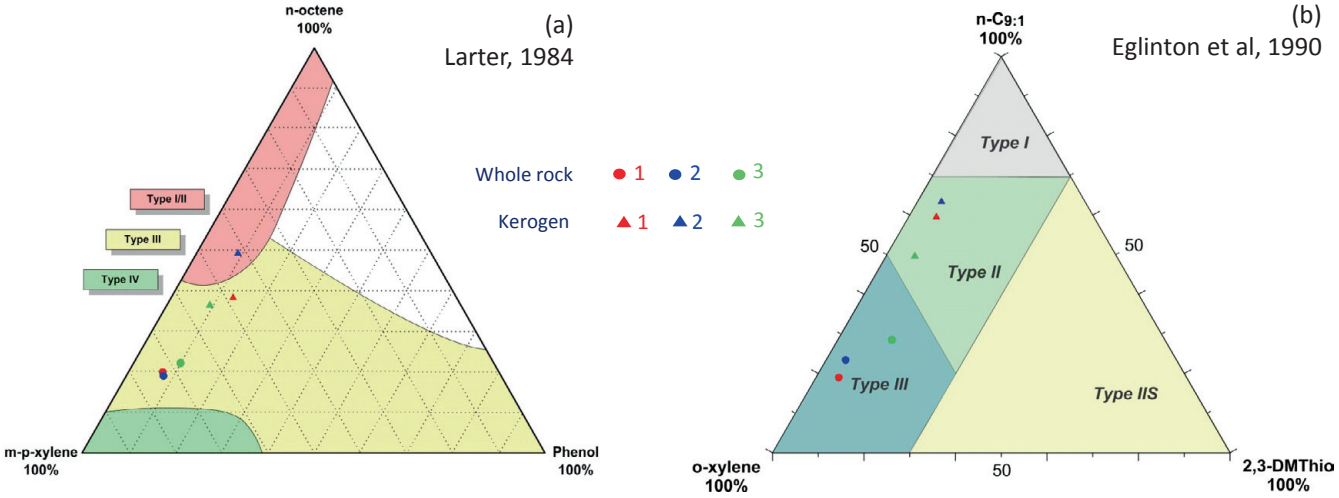


**Fig. 6.** Petroleum composition predictions from PyGC results according to Larter (1984) and Eglinton *et al*. (1990).

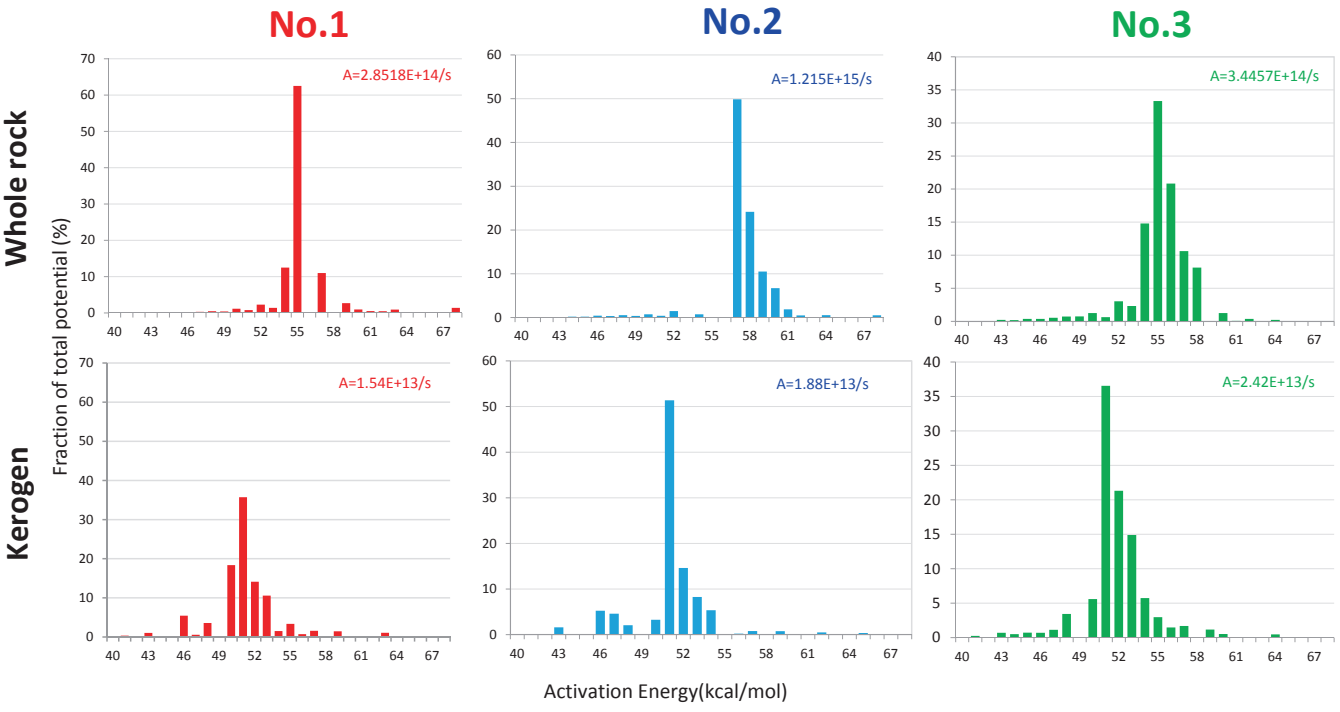


**Fig. 7.** Bulk kinetics models of the whole-rock samples and kerogen concentrates.

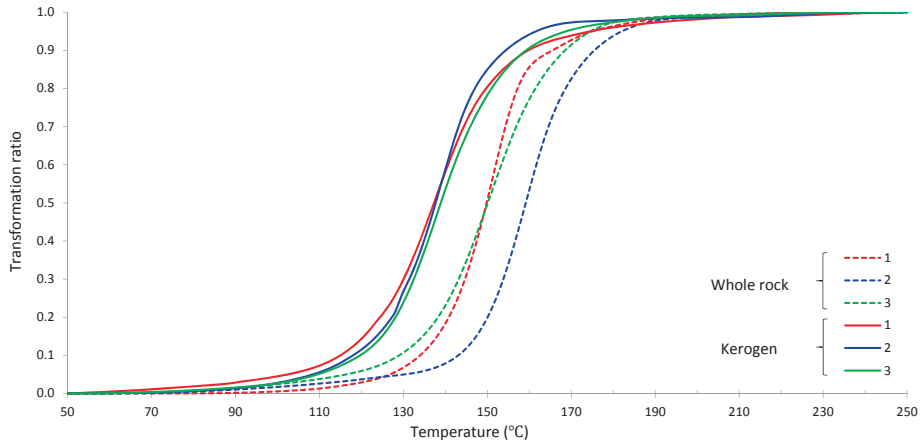


**Fig. 8.** Transformation ratio variations at a geological heating rate of 3°C Ma$^{-1}$.

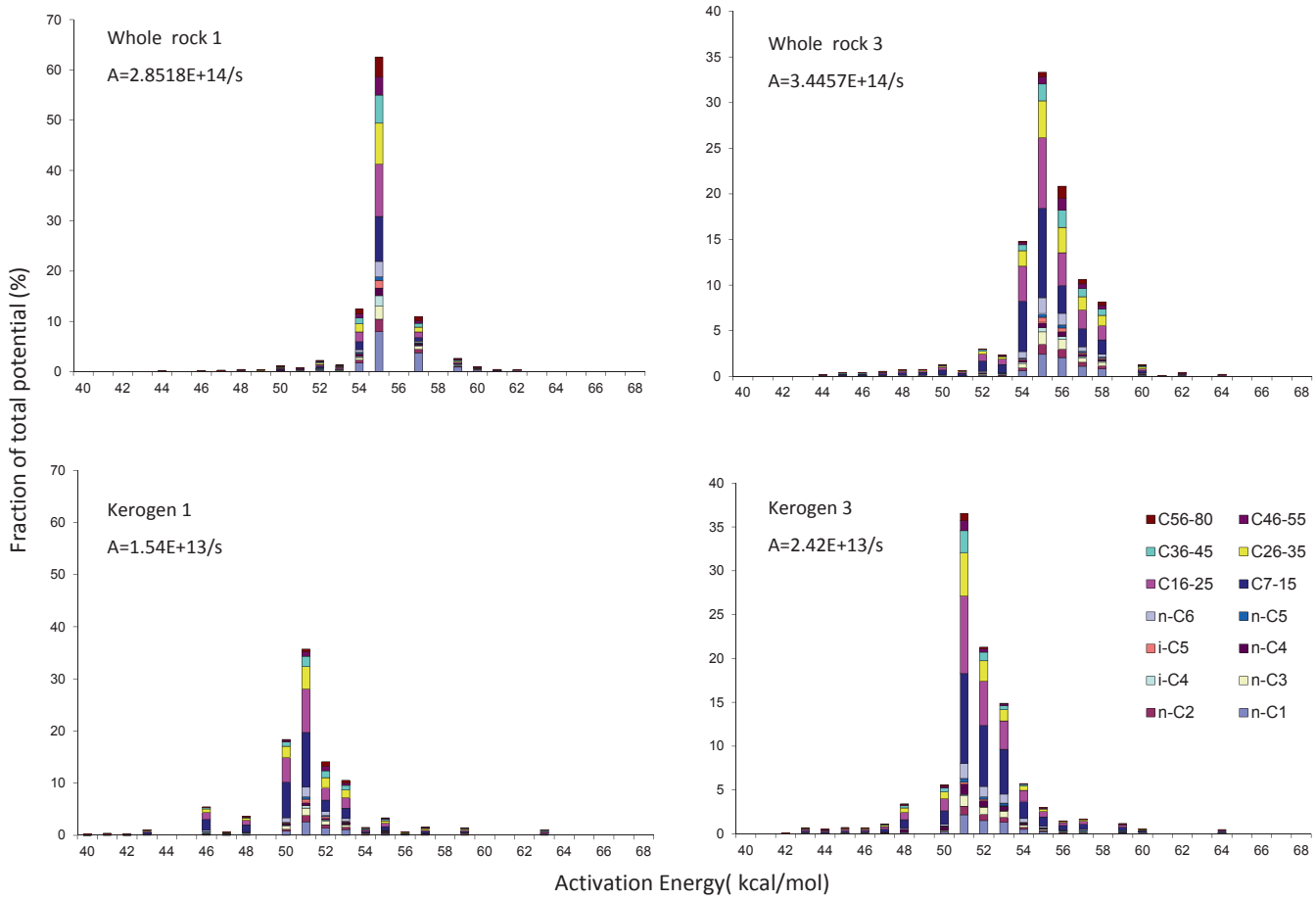


**Fig. 9.** Compositional kinetic models of selected samples.

not every source rock necessarily has to show this effect. Horsfield & Douglas (1980) and Katz (1983) concluded that the matrix effect varies according to mineralogy and TOC content of the rocks under investigation. A very high TOC or low clay content can decrease or prevent the effect (Reynolds *et al.* 1995). Tannenbaum & Kaplan (1985) and Lewan *et al.* (2014) also reported that the existence of water in the pyrolysis experiments can hinder the excessive formation of coke and catalysing function of clay minerals. However, because the TOC content of Bowland Shale ranges from 1.3 to 9.1% (Gross *et al.* 2014), clay contents are considered to be medium to high (USEIA 2011) and all pyrolysis experiments employed here are anhydrous systems, the mineral matrix effect is probably inevitable in the Bowland Shale pyrolysis experiments (except in those samples with TOC content higher than 6%). If whole-rock samples are used in the Bowland Shale PhaseKinetics research here, the cumulative GOR can be greatly overestimated and leads to erroneous conclusions in phase prediction and resource evaluation.

### *Secondary cracking*

GOR-Fit was applied to kerogen 3 to explore the generation characteristics and kinetics of primary oil, primary gas and secondary gas formation. As the MSSV experiments at 5°C min$^{-1}$ heating rate show, the $C_{6+}$ fraction starts to decrease at around 460°C with increasing temperature (Fig. 12) as a result of secondary cracking. The decrease of $C_{1+}$ generation and $C_{1-5}$ products after 510°C and 540°C (Fig. 12) indicates the formation of coke or pyrobitumen (Dieckmann *et al.* 1998). Small-scale secondary cracking occurs when the temperature reaches 420°C in the MSSV, and significantly

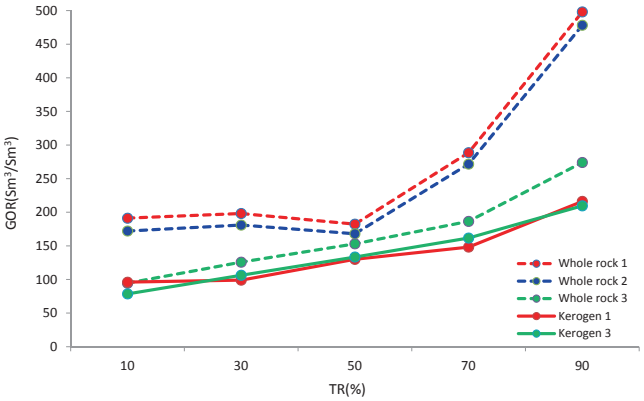


**Fig. 10.** Gas:oil ratio of the samples analysed as a function of increasing transformation ratio.

more secondary gas is formed after 460°C, where the onset of the decrease of $C_{6+}$ compounds in the MSSV occurs (Fig. 12). The excellent identical trends of secondary gas in the MSSV and calculated secondary gas (Fig. 12) attest to the robustness of the GOR-Fit approach.

By combining the generation spline under three heating rates (0.7, 2.0 and 5.0°C min$^{-1}$), the kinetics of primary oil, primary gas and secondary cracking can be accurately drawn (Fig. 13). The activation energy distribution of primary oil (Fig. 13) is very similar to the bulk kinetic distribution (Fig. 7). Compared with primary gas, the peak activation energy of secondary gas is 10 kcal mol$^{-1}$ higher, and the frequency factor is increased by 2° (Fig. 13).

The generation rate of bulk primary hydrocarbons (SRA), primary oil, primary gas and secondary gas at a linear heating rate of 3 K Ma$^{-1}$ is shown in Figure 14. Both the primary oil and gas generation curve are within the SRA range. About 80% of the primary hydrocarbon was contributed by primary oil, and this partly explains why both the SRA and primary oil reach peak generation rates between 136 and 138°C (Fig. 14). When the temperature has reached 150°C and the $R_o$ is 1.2% the primary gas reaches its maximum generation rate. The secondary gas generation capability of the sample is of crucial importance in shale gas potential evaluation, as seen in, for example, the Fort Worth Basin (Jarvie *et al.* 2007). Much higher maturity is required to achieve the secondary gas compared with the primary gas, as the peak secondary generation temperature reaches 200°C, which is 50°C higher than that for primary gas, and vitrinite reflectance is as high as 2.0% (Fig. 14).

## Application

### *Primary generation*

The upper Bowland Shale in well Grove 3 lies in the lower part of Namurian stage and was overlaid by the Millstone Grit. Since the target layer is very thin in the borehole, here we use Namurian layer to represent it in the 1 D basin modelling for illustrative purpose. Modelling results demonstrate that the upper Bowland Shale experienced rapid burial in the late Carboniferous and the kerogen attained about 26% TR at the end of the Carboniferous (roughly equivalent to $R_o$ 0.6%) (Fig. 15a), when the primary generation started (Fig. 14). During this period, the main driving force for hydrocarbon expulsion would be pressure-driven flow as kerogen

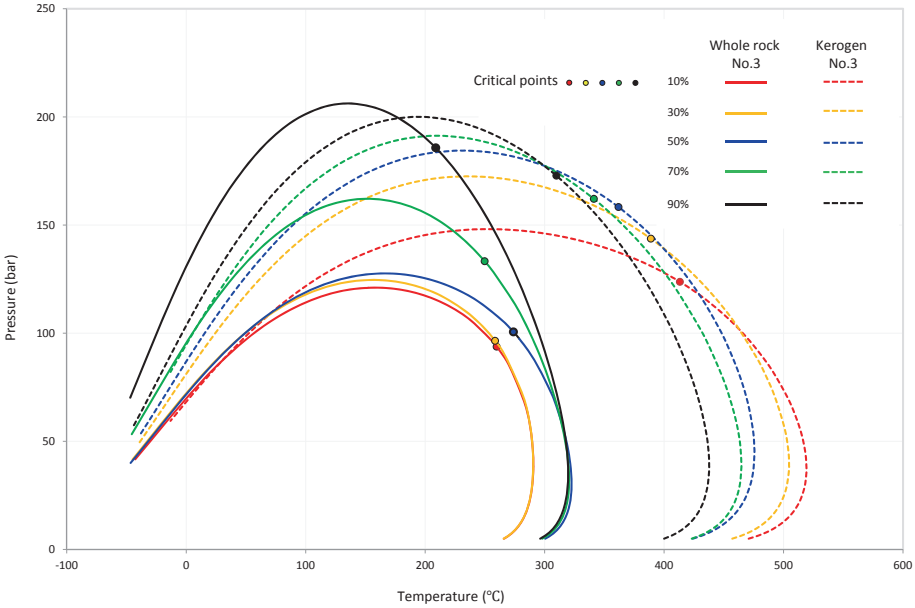


**Fig. 11.** Phase envelopes of whole-rock 3and kerogen 3 during artificial maturation.

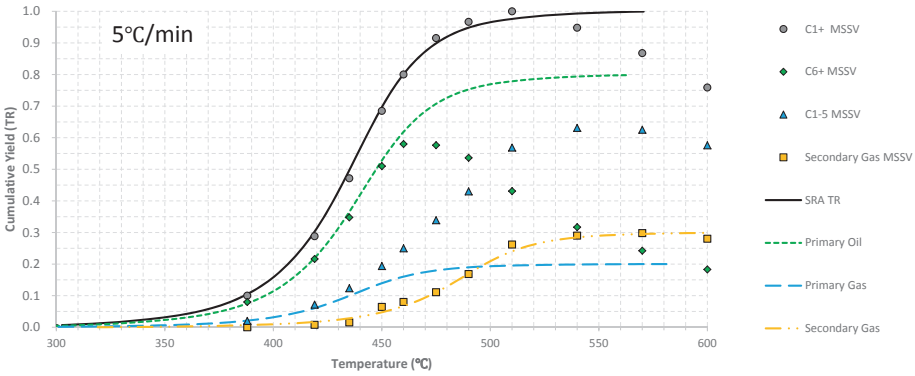


**Fig. 12.** Measured MSSV pyrolysis data of kerogen 3 for boiling ranges $C_{1+}$, $C_{6+}$ and $C_{1-5}$ normalized to the maximum $C_{1+}$ yield and fitted spline curves for calculated primary and secondary gas generation using a heating rate of 5.0°C min$^{-1}$, compared with normalized SRA TR curve.

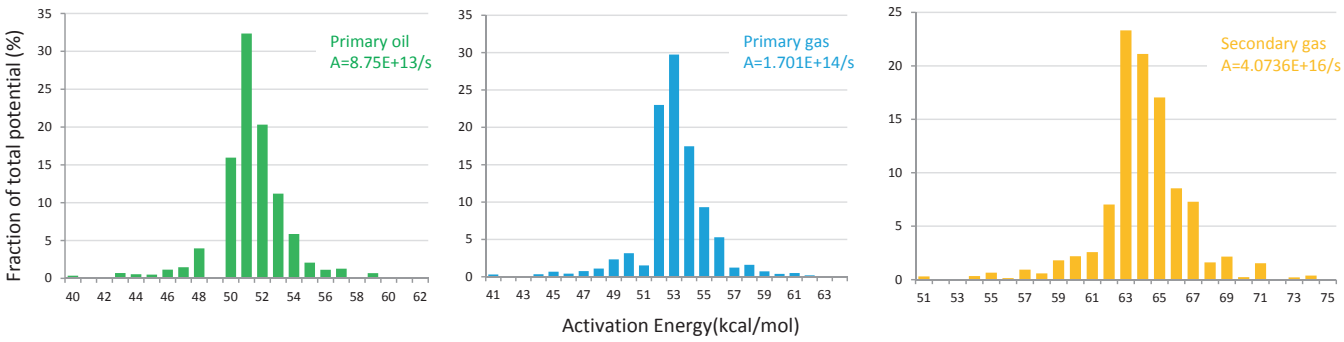


**Fig. 13.** Kinetics models of primary oil, primary gas and secondary gas generation of kerogen 3.

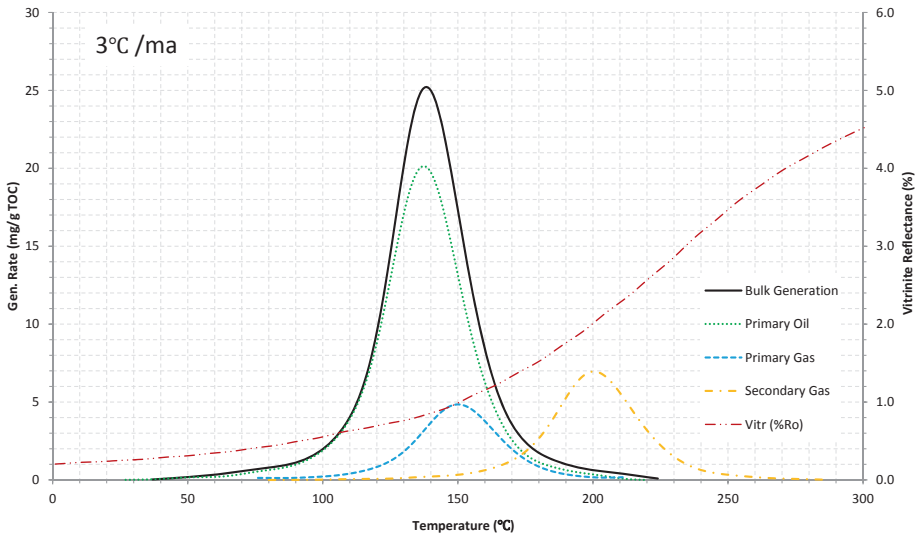


**Fig. 14.** Computed vitrinite reflectance and generation rate curves as a function of temperature at a geological heating rate of 3°C $Ma^{-1}$ and vitrinite reflectance for kerogen 3.

degradation and rapid compaction took place (see Tissot & Welte 1984, p. 323). Fluids generated at TR 30% fall into the one-phase field in reservoir conditions (Fig. 15c), indicating that *in situ* primary hydrocarbons would exist as an undersaturated liquid in the source rock. The uplift that occurred during the late Carboniferous to early Permian not only stopped the rapid organic maturation but also changed the reservoir conditions significantly (point A has a temperature of 90°C and pressure of 186 bar, whereas the temperature and pressure of point B are 51°C and 72 bar, respectively) (Fig. 15a). If we use 30% TR fluids to roughly represent the hydrocarbon generated at point A, it can be predicted that when petroleum in the source rock was shifted from point A to point B the decrease in temperature and pressure would cause a phase separation, and gas composition would contribute 8% in volume of the whole fluids (Fig. 15c). This sudden gas exsolution in the very tight shale reservoir would cause an abnormal pressure in the source rock and greatly increase the expulsion efficiency (see Momper 1979). Thus the driving force for expulsion in this period would be changed to the abnormal pressure caused by volumetric expansion induced by phase separation. Later the shale was deeply buried again between Jurassic and Cretaceous time and the TR of the organic matter became as high as 92% at a maximum burial of 2900 m (Fig. 15a). By the end of the Mesozoic (roughly equivalent to $R_o$ 1.4%) primary generation entered its late stage (Fig. 14). Expulsion would have been driven by continuous burial and vast hydrocarbon generation. A major uplift occurred in the Cenozoic, which again reduced the temperature and pressure of the Bowland Shale reservoir (point C has a temperature of 160°C and pressure of 283 bar, and the temperature and pressure of point D are 73°C and 187 bar). However, this time, phase separation would not be likely to occur during the uplift, when reservoir conditions of TR 90% fluids were changed from point C to point D (Fig. 15f). Practically, if petroleum under reservoir conditions (point D in Fig. 15a and f) was produced to the surface (point E in Fig. 15a and f) a gas exsolution would occur again, and the vapour phase would hold about 25% of the total fluid (Fig. 15f).

In the combination of burial history and phase properties of hydrocarbons generated in geological time, different dominant expulsion driving forces can be proposed and the surface GOR can be assessed. Different expulsion driving forces and mechanisms lead to varying expulsion efficiency and define the amount and property of the unconventional resource left in the source rock. Although only primary hydrocarbon is addressed here, any further secondary cracking, migration or biodegradation would act upon this first-formed composition. The produced GOR prediction is very important in oilfield strategy decision-making, because different fluids vary in terms of economic perspective and engineering requirement. Unfortunately, there are no production data for this well to verify the phase prediction results. Nevertheless, this systematic approach including hydrocarbon composition simulation, phase variation prediction and basin modelling application could be a new approach in unconventional system production prediction and resource evaluation.

### *Secondary cracking*

Kinetics results shown in Figure 13 can be converted as a kerogen–oil–gas kinetics input model in the basin modelling software, thus gas generated under secondary cracking by upper Bowland Shale in well Grove 3 can be simulated (Fig. 16a). The maximum generation of secondary gas is 151169 tons $km^{-2}$ (Table 2) and about 90000 tons in the area (Fig. 16a); however, if a default kerogen–oil–gas kinetics model developed by (Quigley *et al.* (1987) is

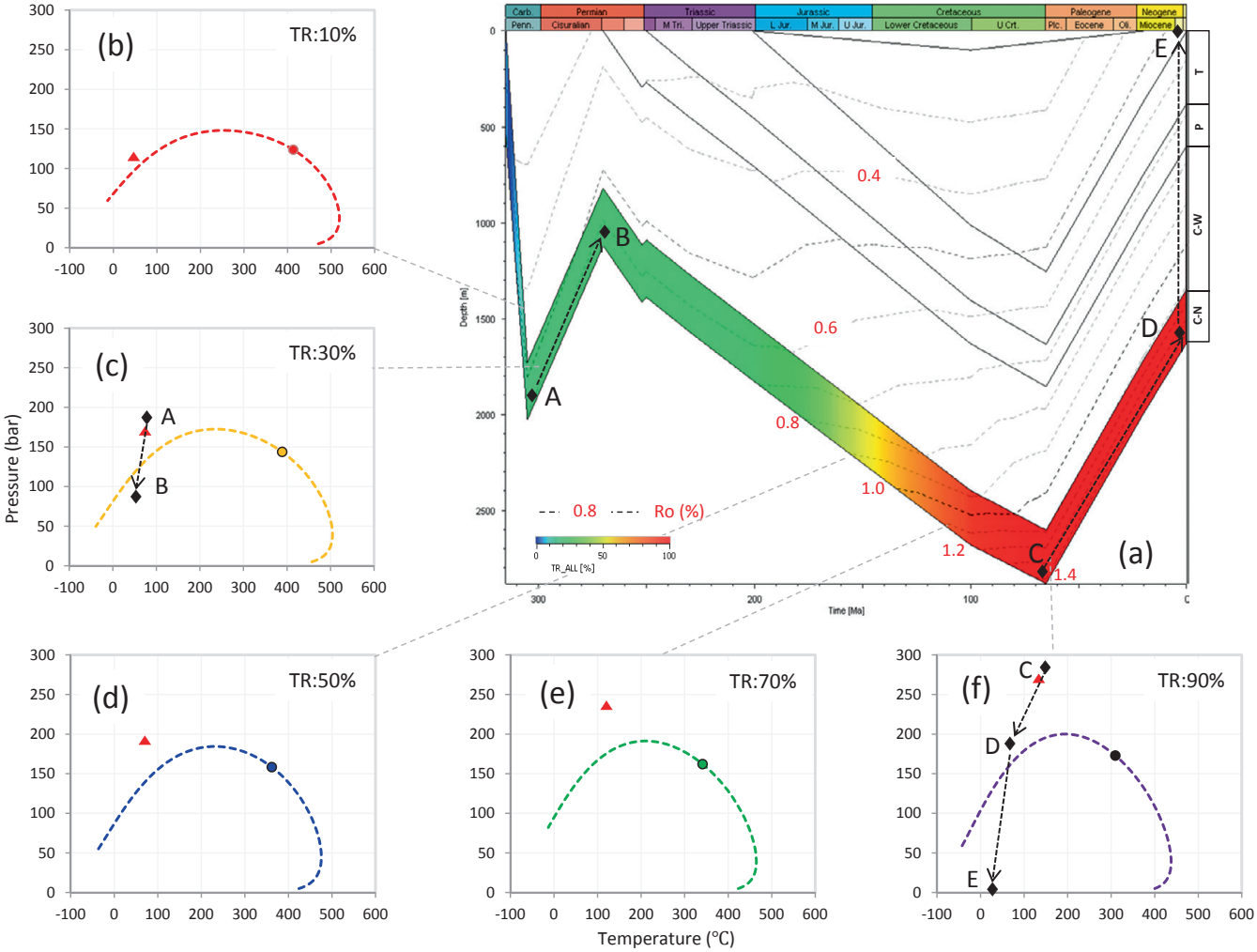


**Fig. 15.** Transformation ratio and $R_o$ evolution histories of well Grove 3 and phase envelopes of primarily generated fluids according to maturity for the upper Bowland Shale. The well location is shown in Figure 1. C-N and C-W in stratigraphy part represent Namurian and Westphalian in Carboniferous respectively. Red trianglein each of the phase envelopes represents reservoir condition in geological burial history. Black diamonds in 1D modelling map and phase envelopes indicate the temperatures and pressures of points A, B, C, D and E, and the black dashed lines linking the points simulate the processes of fluid migration between different reservoir conditions, with the arrows indicating the direction of the movement.

**Table 2.** *Detailed information about default kerogen-oil-gas kinetics models shown in Figure 17*

| Reference | Kerogen type | Lithology | Location of sample | Age of sample | Secondary gas (ton km$^{-2}$) |
|---|---|---|---|---|---|
| Burnham & Sweeney (1989) | II | – | – | – | 3182 |
| Vandenbroucke *et al*. (1999) | II | Shale | North Sea | Kimmeridgian | 5597 |
| Behar *et al*. (1997) | II | Shale | Paris Basin | Toarcian | 8028 |
| Dieckmann *et al*. (2000) | II | Lime mudstones | Western Canada Basin | Upper Devonian | 8226 |
| Quigley *et al*. (1987) | II | – | – | – | 30492 |
| Dieckmann *et al*. (1998) | II | Shale | Lower Saxonian Basin | Toarcian | 101124 |
| Ungerer (1990) | II | Shale | North Sea | Kimmeridgian | 130254 |
| This research | II | Shale | Northern England | Lower Carboniferous | 151169 |
| Pepper & Corvi (1995) | II | Siliciclastic | Mixed | – | 161430 |
| Waples *et al*. (1992) | II | Artificial | – | – | 226920 |

applied, the secondary gas products are predicted to be only 30492 ton km$^{-2}$ (Table 2) and about 20000 tons in the area (Fig. 16b). A more comprehensive comparison of maximum secondary gas generation in Grove 3 predicted by kinetics developed in this study and in nine other type II source rock default kinetics models (Quigley *et al.* 1987, Ungerer 1990; Waples *et al.* 1992; Pepper & Corvi 1995; Behar *et al.* 1997; Dieckmann *et al.* 1998; Abu-Ali *et al.* 1999; Vandenbroucke *et al.* 1999; Dieckmann *et al.* 2000) indicates that the result can vary enormously (Fig. 17; Table 2). A maximum secondary generation of 226920 ton km$^{-2}$ predicted by (Waples *et al.* 1992) is more than 70 times larger than the result of the Burnham & Sweeney (1989) model, which is only 3182 ton km$^{-2}$ (Fig. 17; Table 2). Relatively speaking, the secondary kinetics model developed in this study provides a moderately high production of secondary gas and shares many similarities with the prediction of the Pepper & Corvi (1995) model (Fig. 17; Table 2). It should be noted that the vitrinite reflectance of upper Bowland Shale in well Grove 3 is only 1.4%, which implies that the shale experienced only a low degree of secondary cracking. Thus more significant differences in secondary gas predictions

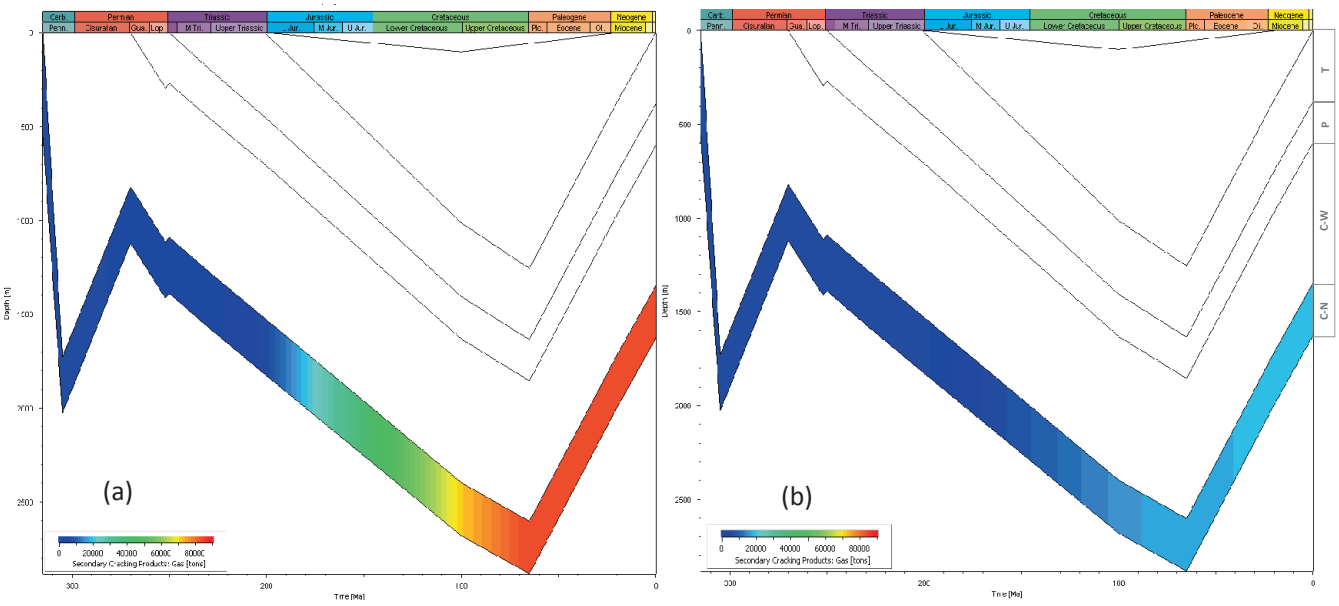


**Fig. 16.** A comparison of secondary gas generation per km$^2$ of upper Bowland Shale in well Grove 3 if (a) the secondary cracking kinetics model of the present study and (b) the kinetics model of Quigley et al. 1987 are applied in the basin modelling.

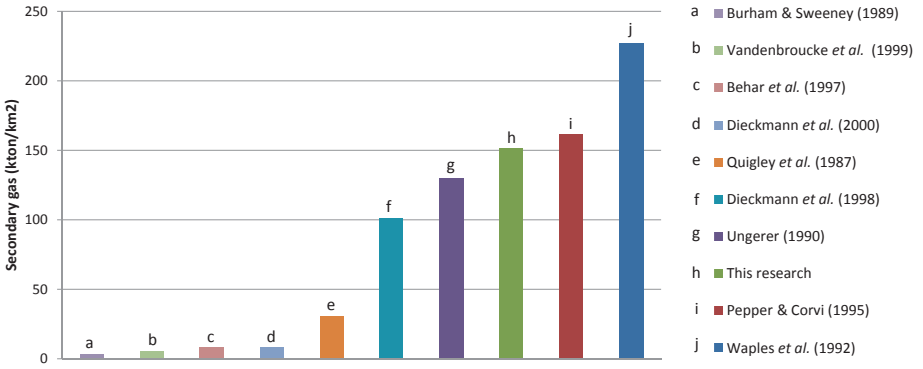


**Fig. 17.** The maximum secondary gas generation per km$^2$ of upper Bowland Shale in well Grove 3 when secondary kinetics of the present study was applied as well as the predictions from 9 other default kerogen–oil–gas kinetic models in PetroMod 2013.

must exist in higher maturity areas when different kinetics models are applied in basin modelling.

Kinetics parameters define in which period of secondary cracking the shale is; for example, a certain maturity may be in the beginning of secondary cracking in one kinetics model but in peak generation in another model. Every target source rock must be approached with a unique secondary kinetics model; huge errors might be induced if default models are selected, and this factor plays a very important role in shale gas in-place assessment.

## Conclusions

Although the mineral matrix effect is a laboratory-induced artefact and may not occur for every shale, the three Bowland Shale samples studied here showed this effect strongly. If whole-rock samples are used in pyrolysis experiments instead of kerogen concentrates, the hydrocarbon generation potential as defined by HI is underestimated, the bulk kinetic parameter indicates higher thermal stabilities, and the inferred natural GOR is overestimated.

The three upper Bowland Shale samples are immature (equivalent $R_o$ less than 0.5%) marine shales and comprise type II kerogen. Kerogens generate pyrolysates diagnostic of paraffinic–naphthenic–aromatic oil with low content of wax and sulphur. The bulk kinetic frequency factors range from $1.54 \times 10^{13}$ to $2.42 \times 10^{13}$ and main activation energies range from 50 to 53 kcal mol$^{-1}$. All these characteristics of Bowland Shale are similar to those of productive Palaeozoic marine shale in the USA such as the Bakken, Barnett and Woodford shales.

The Bowland Shale possesses a high secondary gas generation potential and primary oil, primary gas and secondary gas reach their maximum generation at 137°C, 150°C and 200°C respectively in geological time.

In the combination of phase properties and burial history, different driving forces of expulsion can be proposed and the produced GORs are predicted. Expulsion efficiency varies with the organic maturity and reservoir conditions, and the amount and properties of the unconventional resource left in the source rock change accordingly.

Vast differences can be found in secondary gas amount prediction when varying default kinetics models are chosen, which emphasizes the significance of a targeted secondary kinetics model in shale gas resource basin modelling evaluation.

## Acknowledgements and Funding

The authors thank Ferdinand Perssen for technical assistance. We are also grateful to editors and two anonymous reviewers for their constructive comments and suggestions. This project was funded by China Scholarship Council.

*Scientific editing by Stuart Jones*

## References

Abu-Ali, M., Rudkiewicz, J., McGillivray, J. & Behar, F. 1999. Paleozoic petroleum system of central Saudi Arabia. *GeoArabia*, **4**, 321–336.

Amyx, J., Bass, D. & Whiting, R. 1960. *Petroleum Reservoir Engineering: Physical Properties*. McGraw–Hill, New York.

Andrews, I. 2013. *The Carboniferous Bowland Shale Gas Study: Geology and Resource Estimation*. British Geological Survey for Department of Energy and Climate Change, London.

Armstrong, J.P., Smith, J., D'Elia, V.A.A. & Trueblood, S.P. 1997. The occurrence and correlation of oils and Namurian source rocks in the Liverpool Bay–North Wales area. *In*: Meadows, N.S., Trueblood, S.R., Hardman, N. & Cowan, G. (eds) *Petroleum Geology of the Irish Sea and Adjacent Areas*. Geological Society, London, Special Publications, **124**, 195–211, http://dx.doi.org/10.1144/GSL.SP.1997.124.01.12.

Barrett, P.A. 1988. Early Carboniferous of the Solway Basin: A tectonostratigraphic model and its bearing on hydrocarbon potential. *Marine and Petroleum Geology*, **5**, 271–281, http://dx.doi.org/10.1016/0264-8172(88)90006-2.

Baur, F., Littke, R., Wielens, H., Lampe, C. & Fuchs, T. 2010. Basin modeling meets rift analysis—A numerical modeling study from the Jeanne d'Arc basin, offshore Newfoundland, Canada. *Marine and Petroleum Geology*, **27**, 585–599, http://dx.doi.org/10.1016/j.marpetgeo.2009.06.003.

Behar, F., Vandenbroucke, M., Tang, Y., Marquis, F. & Espitalie, J. 1997. Thermal cracking of kerogen in open and closed systems: Determination of kinetic parameters and stoichiometric coefficients for oil and gas generation. *Organic Geochemistry*, **26**, 321–339.

Bowker, K.A. 2007. Barnett Shale gas production, Fort Worth Basin: Issues and discussion. *AAPG Bulletin*, **91**, 523–533, http://dx.doi.org/10.1306/06190606018.

Braun, R.L. & Burnham, A.K. 1987. Analysis of chemical reaction kinetics using a distribution of activation energies and simpler models. *Energy & Fuels*, **1**, 153–161, http://dx.doi.org/10.1021/ef00002a003.

Burnham, A. 1994. Comments on 'The effects of the mineral matrix on the determination of kinetic parameters using modified Rock-Eval pyrolysis' by H. Dembicki Jr, and the resulting comment. *Organic Geochemistry*, **21**, 985–986.

Burnham, A. & Sweeney, J. 1989. A chemical kinetic model of vitrinite maturation and reflectance. *Geochimica et Cosmochimica Acta*, **53**, 2649–2651.

Burnham, A., Braun, R., Gregg, H. & Samoun, A. 1987. Comparison of methods for measuring kerogen pyrolysis rates and fitting kinetic parameters. *Energy & Fuels*, **1**, 452–458.

Burnham, A.K., Braun, R.L. & Samoun, A.M. 1988. Further comparison of methods for measuring kerogen pyrolysis rates and fitting kinetic parameters. *Organic Geochemistry*, **13**, 839–845, http://dx.doi.org/10.1016/0146-6380(88)90236-7.

Chisholm, J., Charsley, T. & Aitkenhead, N. 1988. *Geology of the Country Around Ashbourne and Cheadle*. HMSO, London.

Cohen, K.M., Finney, S.C., Gibbard, P.L. & Fan, J.-X. 2014. The ICS International Chronostratigraphic Chart. *Episodes*, **36**, 199–204, doi: 10.1111/j.1502-3931.1980.tb01026.x.

Curtis, J. 2002. Fractured shale-gas systems. *AAPG Bulletin*, **11**, 1921–1938.

DECC. 2011. The unconventional hydrocarbon resources of Britain's onshore basins—shale gas. DECC Promote website, December 2010. https://www.gov.uk/government/uploads/system/uploads/attachment_data/file/367287/Shalegas_uk.pdf

Dembicki, J.R. 1992. The effects of the mineral matrix on the determination of kinetic parameters using modified Rock Eval pyrolysis. *Organic Geochemistry*, **18**, 531–539.

de Pater, C. & Baisch, S. 2011. *Geomechanical study of Bowland Shale seismicity. Synthesis Report*, http://www.cuadrillaresources.com/wp-content/uploads/2012/02/Geomechanical-Study-of-Bowland-Shale-Seismicity_02-11-11.pdf

Dessort, D., Connan, J., Derenne, S. & Largeau, C. 1997. Comparative studies of the kinetic parameters of various algaenans and kerogens via open-system pyrolyses. *Organic Geochemistry*, **26**, 705–720, http://dx.doi.org/10.1016/S0146-6380(97)00038-7.

Dieckmann, V. 2005. Modelling petroleum formation from heterogeneous source rocks: The influence of frequency factors on activation energy distribution and geological prediction. *Marine and Petroleum Geology*, **22**, 375–390, http://dx.doi.org/10.1016/j.marpetgeo.2004.11.002.

Dieckmann, V. & Keym, M. 2006. A new approach to bridge the effect of organofacies variations on kinetic modelling and geological extrapolations. *Organic Geochemistry*, **37**, 728–739, http://dx.doi.org/10.1016/j.orggeochem.2005.12.008.

Dieckmann, V., Schenk, H., Horsfield, B. & Welte, D. 1998. Kinetics of petroleum generation and cracking by programmed-temperature closed-system pyrolysis of Toarcian Shales. *Fuel*, **77**, 23–31.

Dieckmann, V., Schenk, H. & Horsfield, B. 2000. Assessing the overlap of primary and secondary reactions by closed- versus open-system pyrolysis of marine kerogens. *Journal of Analytical and Applied Pyrolysis*, **56**, 33–46, http://dx.doi.org/10.1016/S0165-2370(00)00083-8.

Di Primio, R. & Horsfield, B. 2006. From petroleum-type organofacies to hydrocarbon phase prediction. *AAPG Bulletin*, **90**, 1031–1058, http://dx.doi.org/10.1306/02140605129.

Di Primio, R., Dieckmann, V. & Mills, N. 1998. *PVT* and phase behaviour analysis in petroleum exploration. *Organic Geochemistry*, **29**, 207–222.

Eglinton, T.I., Sinninghe Damsté, J.S., Kohnen, M.E.L. & de Leeuw, J.W. 1990. Rapid estimation of the organic sulphur content of kerogens, coals and asphaltenes by pyrolysis–gas chromatography. *Fuel*, **69**, 1394–1404, http://dx.doi.org/10.1016/0016-2361(90)90121-6.

Espitalié, J., Madec, M., Tissot, B.P., Mennig, J.J. & Leplat, P. 1977. Source rock characterization method for petroleum exploration. *In*: *Offshore Technology Conference, Houston*, 439–444.

Espitalie, J., Madec, M. & Tissot, B. 1980. Role of mineral matrix in kerogen pyrolysis: Influence on petroleum generation and migration. *AAPG Bulletin*, 59–66.

Espitalié, J., Makadi, K.S. & Trichet, J. 1984. Role of the mineral matrix during kerogen pyrolysis. *Organic Geochemistry*, **6**, 365–382.

Ewbank, G., Manning, D. & Abbott, G. 1993. An organic geochemical study of bitumens and their potential source rocks from the South Pennine Orefield, Central England. *Organic Geochemistry*, **20**, 579–598.

Fraser, A. & Gawthorpe, R. 2003. *An Atlas of Carboniferous Basin Evolution in Northern England*. Geological Society, London, Memoirs, **28**, http://dx.doi.org/10.1144/GSL.MEM.2003.028.01.08.

Gradstein, F., Ogg, J. & Smith, A. 2004. *A Geologic Time Scale 2004*. Cambridge University Press, Cambridge.

Green, C., Styles, P. & Baptie, B. 2012. *Preese Hall Shale Gas Fracturing Review and Recommendations for Induced Seismic Mitigation*. Department of Energy and Climate Change, London.

Gross, D., Sachsenhofer, R.F., Bechtel, A., Pytlak, L., Rupprecht, B. & Wegerer, E. 2014. Organic geochemistry of Mississippian shales (Bowland Shale Formation) in central Britain: Implications for depositional environment, source rock and gas shale potential. *Marine and Petroleum Geology*, **59**, 1–21, http://dx.doi.org/10.1016/j.marpetgeo.2014.07.022.

Hartwig, A., di Primio, R., Anka, Z. & Horsfield, B. 2012. Source rock characteristics and compositional kinetic models of Cretaceous organic rich black shales offshore southwestern Africa. *Organic Geochemistry*, **51**, 17–34, http://dx.doi.org/10.1016/j.orggeochem.2012.07.008.

Horsfield, B. 1989. Practical criteria for classifying kerogens: Some observations from pyrolysis–gas chromatography. *Geochimica et Cosmochimica Acta*, **53**, 891–901.

Horsfield, B. 1997. The bulk composition of first-formed petroleum in source rocks. *In:* Welte, D.H., Horsfield, B. & Baker, D.R. (eds) *Petroleum and Basin Evolution*. Springer, Berlin, 337–402.

Horsfield, B. & Douglas, A.G. 1980. The influence of minerals on the pyrolysis of kerogens. *Geochimica et Cosmochimica Acta*, **44**, 1119–1131.

Horsfield, B., Disko, U. & Leistner, F. 1989. The micro-scale simulation of maturation: Outline of a new technique and its potential applications. *Geologische Rundschau*, **78**, 361–373, http://dx.doi.org/10.1007/BF01988370.

Horsfield, B., Leistner, F. & Hall, K. 2015. Microscale sealed vessel pyrolysis. *In:* Grace, K. (ed.) *Principles and Practice of Analytical Techniques in Geosciences*. Royal Society of Chemistry, Cambridge, UK, 209–250.

Hough, E. & Vane, C. 2014. The Bowland Shale in the Roosecote Borehole of the Lancaster Fells Sub-Basin, Craven Basin, UK: a potential UK shale gas play? *SPE–EAGE European Unconventional Resources Conference and Exhibition, Vienna, Austria, 25–27 February*, 25–27. http://www.earthdoc.org/publication/publicationdetails/?publication=75097

Imber, J., Armstrong, H. & Clancy, S. 2014. Natural fractures in a UK shale reservoir analogue, Cleveland Basin, northeast England, *AAPG Bulletin*, **98**, 2411–2437, http://dx.doi.org/10.1306/07141413144.

Jarvie, D.M., Hill, R.J., Ruble, T.E. & Pollastro, R.M. 2007. Unconventional shale-gas systems: The Mississippian Barnett Shale of north–central Texas as one model for thermogenic shale-gas assessment. *AAPG Bulletin*, **91**, 475–499, http://dx.doi.org/10.1306/12190606068.

Jarvie, D., Behar, F. & Mazéas, L. 2010. Decomposition of organic matter and impact on shale resource play assessments. *AAPG Annual Convention and Exhibition, New Orleans, LA, 11–14 April*. http://www.searchanddiscovery.com/pdfz/documents/2010/110125jarvie/ndx_jarvie.pdf.html

Jarvis, G.T. & McKenzie, D.P. 1980. Sedimentary basin formation with finite extension rates. *Earth and Planetary Science Letters*, **48**, 42–52, http://dx.doi.org/10.1016/0012-821X(80)90168-5.

Karabakan, A. & Yürüm, Y. 1998. Effect of the mineral matrix in the reactions of oil shales: 1. Pyrolysis reactions of Turkish Göynük and US Green River oil shales. *Fuel*, **77**, 1303–1309.

Katz, B.J. 1983. Limitations of 'Rock-Eval' pyrolysis for typing organic matter. *Organic Geochemistry*, **4**, 195–199, http://dx.doi.org/10.1016/0146-6380(83)90041-4.

Könitzer, S.F., Davies, S.J., Stephenson, M.H. & Ko, S.F. 2014. Depositional controls on mudstone lithofacies in a basinal setting: Implications for the delivery of sedimentary organic matter. *Journal of Sedimentary Research*, **84**, 198–214.

Kuhn, P.P., di Primio, R., Hill, R., Lawrence, J.R. & Horsfield, B. 2012. Three-dimensional modeling study of the low-permeability petroleum system of the Bakken Formation. *AAPG Bulletin*, **96**, 1867–1897, http://dx.doi.org/10.1306/03261211063.

Larter, S.R. 1984. Application of analytical pyrolysis techniques to kerogen characterization and fossil fuels exploration/exploitation. *In:* Voorhes, K.J. (ed.) *Analytical Pyrolysis Techniques and Applications*. Butterworths, London, 212–275.

Lawrence, S.R., Coster, P.W. & Ireland, R.J. 1987. Structural development and petroleum potential of the northern flanks of the Craven Basin (Carboniferous), North West England. *In*: Brooks, J. & Glennie, K.W. (eds) *Petroleum Geology of North West Europe*. Graham & Trotman, London, 225–233.

Leeder, M.R. 1988. Recent developments in Carboniferous geology: A critical review with implications for the British Isles and N.W. Europe. *Proceedings of the Geologists' Association*, **99**, 73–100, http://dx.doi.org/10.1016/S0016-7878(88)80001-4.

Lewan, M.D., Dolan, M.P. & Curtis, J.B. 2014. Effects of smectite on the oil-expulsion efficiency of the Kreyenhagen Shale, San Joaquin Basin, California, based on hydrous-pyrolysis experiments. *AAPG Bulletin*, **98**, 1091–1109, http://dx.doi.org/10.1306/10091313059.

Lu, S., Ruth, E. & Kaplan, I. 1989. Pyrolysis of kerogens in the absence and presence of montmorillonite—I. The generation, degradation and isomerization of steranes and triterpanes at 200 and 300°C. *Organic Geochemistry*, **14**, 491–499.

Mahlstedt, N.L. 2012. *Evaluating the late gas potential of source rocks stemming from different sedimentary environments*. Genehmigte PhD dissertation, Technical University of Berlin.

Mahlstedt, N., di Primio, R. & Horsfield, B. 2013. GOR-Fit—from liquids to late gas: deconvoluting primary from secondary gas generation kinetics. *In*: *Book of Abstracts of the Communications, 26th International Meeting on Organic Geochemistry—IMOG, Costa Adeje, Tenerife, Spain, 15–20 September*, 193–194.

McCain, W.D. 1990. *The Properties of Petroleum Fluids*. PennWell Books, Tulsa, OK.

Momper, J. 1979. Domestic oil reserves forecasting method and assessment of regional potentials. *AAPG Bulletin*, **63**, 497–498.

Muntendam-Bos, A. 2009. Inventory non-conventional gas. *TNO Built Environment and Geosciences*, https://www.ebn.nl/wp-content/uploads/2014/11/200909_Inventory_non-conventional_gas.pd

Pelet, R. 1994. Comments on the paper 'The effects of the mineral matrix on the determination of kinetic parameters using modified Rock-Eval pyrolysis' by H. Dembicki Jr. *Organic Geochemistry*, **21**, 979–981.

Pepper, A.S. & Corvi, P.J. 1995. Simple kinetic models of petroleum formation. Part I: Oil and gas generation from kerogen. *Marine and Petroleum Geology*, **12**, 291–319.

Peters, K.E., Walters, C.C. & Mankiewicz, P.J. 2006. Evaluation of kinetic uncertainty in numerical models of petroleum generation. *AAPG Bulletin*, **90**, 387–403, http://dx.doi.org/10.1306/10140505122.

Pollastro, R.M. 2007. Total petroleum system assessment of undiscovered resources in the giant Barnett Shale continuous (unconventional) gas accumulation, Fort Worth Basin, Texas. *AAPG Bulletin*, **91**, 551–578, http://dx.doi.org/10.1306/06200606007.

Quigley, T., MacKenzie, A. & Gray, J. 1987. Kinetic theory of petroleum generation. *Collection colloques et séminaires-Institut français du pétrole*, **45**, 649–665.

Raji, M. 2013. Unconventional oil and gas potential of the Widmerpool Gulf in the East Midlands Province of England. *In*: *Unconventional Resources Technology Conference, Denver, CO, 12–14 August*. http://archives.datapages.com/data/urtec/2013/urtec-1579451-raji.htm?q=%2BtextStrip%3Ashale+textStrip%3Agas

Reynolds, J., Burnham, A. & Mitchell, T. 1995. Kinetic analysis of California petroleum source rocks by programmed temperature micropyrolysis. *Organic Geochemistry*, **23**, 109–120.

Robl, T. & Davis, B. 1993. Comparison of the HF–HCl and HF–$BF_3$ maceration techniques and the chemistry of resultant organic concentrates. *Organic Geochemistry*, **20**, 249–255.

Rodrigues Duran, E., di Primio, R., Anka, Z., Stoddart, D. & Horsfield, B. 2013. 3D-basin modelling of the Hammerfest Basin (southwestern Barents Sea): A quantitative assessment of petroleum generation, migration and leakage. *Marine and Petroleum Geology*, **45**, 281–303, http://dx.doi.org/10.1016/j.marpetgeo.2013.04.023.

Saxby, J.D. 1970. Isolation of kerogen in sediments by chemical methods. *Chemical Geology*, **6**, 173–184, http://dx.doi.org/10.1016/0009-2541(70)90017-3.

Schenk, H. & Horsfield, B. 1993. Kinetics of petroleum generation by programmed-temperature closed- versus open-system pyrolysis. *Geochimica et Cosmochimica Acta*, **57**, 623–630, http://dx.doi.org/10.1016/0016-7037(93)90373-5.

Schenk, H., Horsfield, B. & Krooss, B. 1997. Kinetics of petroleum formation and cracking. *In*: Welte, D.H., Horsfield, B. & Baker, D.R. (eds) *Petroleum and Basin Evolution*. Springer, Berlin, 231–269.

Selley, R.C. 1987. British shale gas potential scrutinized. *Oil and Gas Journal*, **85**, 62–64.

Selley, R.C. 2005. UK shale-gas resources. *In*: Doré, A.G. & Vining, B.A. (eds) *Geological Society, London, Petroleum Geology Conference Series*, **6**, 707–714, http://dx.doi.org/10.1144/0060707.

Selley, R.C. 2012. UK shale gas: The story so far. *Marine and Petroleum Geology*, **31**, 100–109, http://dx.doi.org/10.1016/j.marpetgeo.2011.08.017.

Senga-Makadi, K. 1982. *Etude Expérimentale des Interactions entre Matière Organique*. PhD dissertation, Université d'Orléans.

Sing, K. 1985. Reporting physisorption data for gas/solid systems with special reference to the determination of surface area and porosity (Recommendations 1984). *Pure and Applied Chemistry*, **57**, 603–619.

Smith, N. 1995. Unconventional hydrocarbons: Changing exploration strategies. *Earthwise*, **7**, 14–15.

Smith, N., Turner, P. & Williams, G. 2010. UK data and analysis for shale gas prospectivity. *In*: Vining, B.A. & Pickering, S.C. (eds) *Geological Society, London, Petroleum Geology Conference Series*, **7**, 1087–1098, http://dx.doi.org/10.1144/0071087.

Tan, J., Horsfield, B. *et al*. 2013. Physical properties of petroleum formed during maturation of Lower Cambrian shale in the upper Yangtze Platform, South China, as inferred from PhaseKinetics modelling. *Marine and Petroleum Geology*, **48**, 47–56, doi: 10.1016/j.marpetgeo.2013.07.013.

Tannenbaum, E. & Kaplan, I. 1985. Low-$M_r$ hydrocarbons generated during hydrous and dry pyrolysis of kerogen. *Nature*, **317**, 708–709.

Tannenbaum, E., Ruth, E. & Kaplan, I.R. 1986. Steranes and triterpanes generated from kerogen pyrolysis in the absence and presence of minerals. *Geochimica et Cosmochimica Acta*, **50**, 805–812.

Tissot, B. & Welte, D. 1984. *Petroleum Formation and Occurrence*. Springer, Berlin.

Ungerer, P. 1990. State of the art of research in kinetic modelling of oil formation and expulsion. *Organic Geochemistry*, **16**, 1–25, http://dx.doi.org/10.1016/0146-6380(90)90022-R.

USEIA. 2011. *World Shale Gas Resources: An Initial Assessment of 14 Regions Outside the United States*. US Energy Information Administration, Washington, DC.

Vandenbroucke, M. & Largeau, C. 2007. Kerogen origin, evolution and structure. *Organic Geochemistry*, **38**, 719–833, http://dx.doi.org/10.1016/j.orggeochem.2007.01.001.

Vandenbroucke, M., Behar, F. & Rudkiewicz, J.L. 1999. Kinetic modelling of petroleum formation and cracking: Implications from the high pressure/high temperature Elgin Field (UK, North Sea). *Organic Geochemistry*, **30**, 1105–1125, http://dx.doi.org/10.1016/S0146-6380(99)00089-3.

Waples, D., Suizu, M. & Kamata, H. 1992. The art of maturity modeling. Part 2: Alternative models and sensitivity analysis. *AAPG Bulletin*, **76**, 47–66.

Waters, C., Waters, R., Barclay, W. & Davies, J. 2009. *A Lithostratigraphical Framework for the Carboniferous Successions of Southern Great Britain (Onshore)*. BGS Report, RR/09/01.

Ziegs, V. 2013. *Development of a compositional kinetic model for primary and secondary petroleum generation from Lower Cretaceous Wealden Shales, Lower Saxony Basin, Northern Germany*. Master Thesis, Technical University of Berlin.